applied sciences

MDPI

Article

Design of N-Way Wilkinson Power Dividers with New Input/Output Arrangements for Power-Halving Operations

Ceyhun Karpuz [1], Mehmet Cakir [1,*], Ali Kursad Gorur [2] and Adnan Gorur [3]

[1] Department of Electrical-Electronics Engineering, Pamukkale University, Denizli 20070, Turkey; ckarpuz@pau.edu.tr
[2] Department of Electrical-Electronics Engineering, Nevsehir Haci Bektas Veli University, Nevsehir 50300, Turkey; kgorur@nevsehir.edu.tr
[3] Department of Electrical and Electronics Engineering, Nigde Omer Halisdemir University, Nigde 51100, Turkey; adnangorur@hotmail.com
* Correspondence: cakirmehmet@pau.edu.tr

Abstract: In this paper, new single/double-layer N-way Wilkinson power dividers (WPDs) were designed by using slow-wave structures such as narrow-slit-loaded and meandered transmission lines. For size reduction, the slit-loaded and meandered lines were used instead of the quarter-wavelength transmission lines of a conventional WPD. Based on the proposed approaches, two-, four-, and eight-way power dividers were designed, simulated, and fabricated. The fabricated 2-, 4-, and 8-way circuits were measured at the center frequencies of 2.03, 1.77, and 1.73 GHz, which are in excellent agreement with the predicted ones. The meandered transmission lines were also used to design WPD types with novel input/output port arrangements. For this purpose, two three-way WPDs were located on both sides of the same board to have different power-splitting ratios at different inputs and outputs in order to provide alternative solutions for antenna arrays. Furthermore, a five-way dual-layer WPD was introduced by locating the meandered transmission lines into two layers. The most important advantage of the proposed 3- and 5-way WPDs is that they allowed the input power at the next output port to be halved, in the order of P/2, P/4, P/8, P/16, and P/16. All the designed power-halving WPDs were simulated, fabricated, and successfully tested.

Keywords: N-way; Wilkinson power dividers (WPDs); meandered transmission line; power halving

Citation: Karpuz, C.; Cakir, M.; Gorur, A.K.; Gorur, A. Design of N-Way Wilkinson Power Dividers with New Input/Output Arrangements for Power-Halving Operations. *Appl. Sci.* **2023**, *13*, 6852. https://doi.org/10.3390/app13116852

Academic Editors: Yating Yu and Baolin Nie

Received: 9 May 2023
Revised: 30 May 2023
Accepted: 1 June 2023
Published: 5 June 2023

1. Introduction

There are different design approaches for WPDs, such as tapered transmission lines [1], three-section [2], dual-band structures [3], dual-lines [4], and triple lines [5]. In addition to these, open-/short-circuited stubs and defected ground structures are used to achieve improved isolation [6–8]. Single- or multi-band WPDs operating in a wide frequency band have also been studied. Among these, semi-lumped-element power dividers with dual-band characteristics in the UHF/SHF bands [9], flexible design schemes for single− and dual−band power-dividing operations [10], dual-band unequal WPDs [11], multi-T-section characterization of high-impedance transmission lines [12], multi-band reconfigurable differential power dividers [13], multiband WPDs based on multisection LC ladder circuits [14], and single/multi-band WPDs with transversal filtering sections [15] stand out. Such WPDs may find application areas especially in multifunctional communication systems. Moreover, the placement of power dividers in antenna arrays is one of the main focuses for researchers. Therefore, size reduction is another important parameter for WPDs, since it is required for feeding the elements of the antenna array within a relatively reduced area. To date, slow-wave structures have been especially used for size reduction. For this purpose, capacitively loaded stubs [16,17] and narrow-slit-loaded and meandered transmission lines [18,19] are largely employed for WPD designs. Periodically, loaded slow-wave structures are modified for different targets, including dual-band applications [20,21], SiGe

BiCMOS processes [22], filtering power dividers having resonant LC branches [23], etc. In some structures, coupled lines are used to suppress undesirable harmonics so that the signal can be transmitted within the desired frequency region [24]. On the other hand, in order to adjust the directivity, antenna array elements may need different power ratios at different elements. Therefore, unequal power dividers may also find applications in antenna arrays to meet the asymmetric power division requirement [25–27]. There are two types of equal WPDs: N-way and cascaded models. N-way WPDs have an input port and N output ports with the impedance of $Z_0\sqrt{2}$, whereas cascaded model WPDs divide the input power by 2 at each cascaded path [28].

In this paper, two-, four-, and eight-way cascaded WPDs are designed by using slow-wave structures. For this purpose, the two-, four-, and eight-way WPDs constructed by using narrow-slit-loaded transmission lines in [28] were first taken into account. Next, they were replaced with meandered transmission lines to improve the compactness. Two-, four-, and eight-way WPDs having meandered transmission lines were also fabricated and successfully measured for demonstration. Based on the meandered transmission lines, three- and five-way WPDs with new input/output port arrangements were designed, fabricated, and successfully measured for demonstration. The proposed three- and five-way circuits allow halving the input power at the next output port.

2. Materials and Methods

2.1. Analysis of WPDs

The S-parameters of a WPD can be calculated by using even–odd mode analysis. An equivalent circuit model for a conventional 2-way WPD is shown in Figure 1a. As can be seen from the figure, quarter-wavelength transmission lines having characteristic impedances of $Z_0\sqrt{2}$ are used in both output paths. Furthermore, an isolation resistor of $2Z_0$ is located between the two output ports. Based on this model, slow-wave transmission lines can be employed instead of the conventional quarter-wavelength transmission lines. Therefore, these models are the starting point of the entire design procedure.

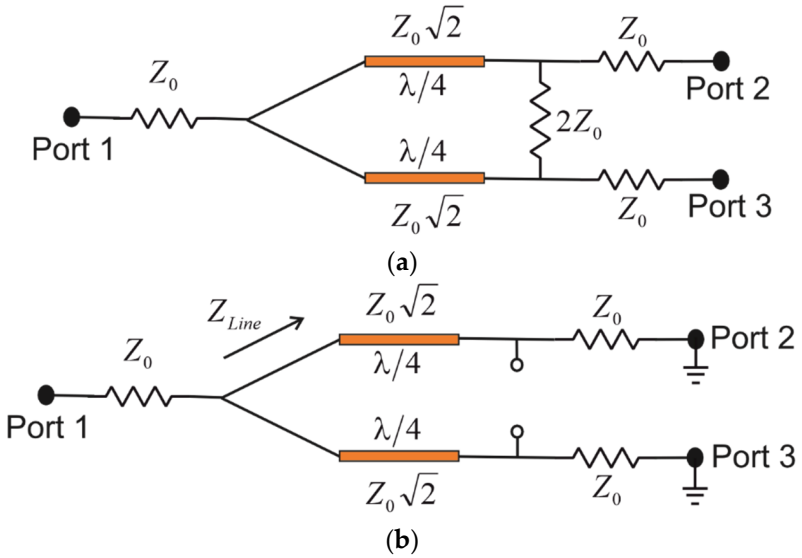

Figure 1. (**a**) Equivalent circuit model of a 2-way WPD. (**b**) Equivalent circuit model for the calculation of S_{11}.

The S parameters of the WPD given in Figure 1a can be obtained by different approaches. In order to obtain S_{11}, the circuit model should be considered as illustrated in

Figure 1b, since no current will flow through the isolation resistor. As can be seen from Figure 1b, S_{11} can be calculated from the following set of equations:

$$S_{11} = \frac{Z_{in} - Z_0}{Z_{in} + Z_0} \tag{1}$$

$$Z_{in} = \frac{Z_{Line}}{2} \tag{2}$$

$$Z_{Line} = Z_0\sqrt{2}\frac{Z_0 + jZ_0\sqrt{2}\tan\theta}{Z_o\sqrt{2} + jZ_0\tan\theta} \tag{3}$$

$$\theta = \frac{2\pi}{\lambda}.\frac{\lambda_0}{4} \tag{4}$$

For equal power splitting, S_{21} and S_{31} can be obtained from S_{11}. Furthermore, the isolation between the output ports can be calculated by using even–odd mode analysis. For this purpose, the even- and odd-mode half-circuits can be obtained by locating the magnetic and electric walls, respectively, on the symmetry axis shown in Figure 2a. Figure 2b,c illustrate the even- and odd-mode half-circuit models, respectively. It should be noted that the isolation resistor can be neglected for the even-mode circuit since the symmetry axis is open-circuited. In addition, the isolation resistor is Z_0 for the odd-mode circuit due to the short-circuited symmetry axis. The isolation between the output ports, S_{32}, can be found by deriving the even-mode and odd-mode input impedances. Here, the circuit model shown in Figure 1a should be considered a 2-port network, with the input port as port 2 and the output port as port 3. Thus, under the even- and odd-mode excitations, the input impedance seen from port 2 or 3 will be the even- and odd-mode input impedances, so that the isolation can be expressed as

$$S_{32} = \frac{(Z_{even} - Z_{odd})Z_0}{(Z_{even} - Z_0)(Z_0 + Z_{odd})} \tag{5}$$

The even-mode input impedance shown in Figure 2b can be expressed as

$$Z_{even} = Z_0\sqrt{2}\frac{2Z_0 + jZ_0\sqrt{2}\tan\theta}{Z_o\sqrt{2} + jZ_0\tan\theta} \tag{6}$$

The odd-mode input impedance can be calculated as

$$Z_{odd} = \frac{Z_xZ_0}{Z_x + Z_0} \tag{7}$$

$$Z_x = jZ_0\sqrt{2}\tan\theta \tag{8}$$

Similar analyses can also be applied to 4- and 8-way WPDs. Since 2 and 3 quarter-wavelength transmission lines should be used in each output path for 4- and 8-way WPDs, respectively, they will excite 2 and 3 transmission poles within the power-dividing frequency band.

2.2. N-Way Wilkinson Power Dividers Based on Slow-Wave Structures

As is well known, 1-to-N-way WPDs consist of N branches which have characteristic impedances of $Z_0\sqrt{N}$, as shown Figure 3. Although they provide better size reduction than that of the cascaded structures, they suffer from the narrow band and poor isolation between output ports [28].

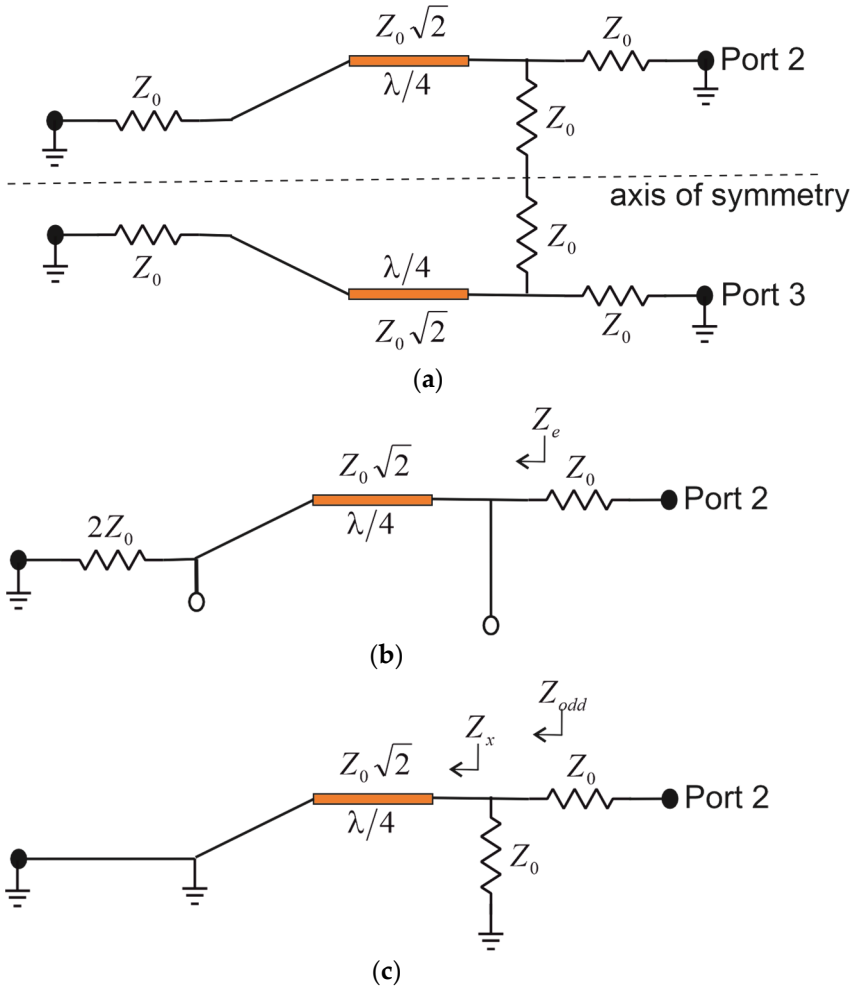

Figure 2. (**a**) Equivalent circuit model for the calculation of S_{32}. (**b**) Even-mode half-circuit model. (**c**) Odd-mode half-circuit model.

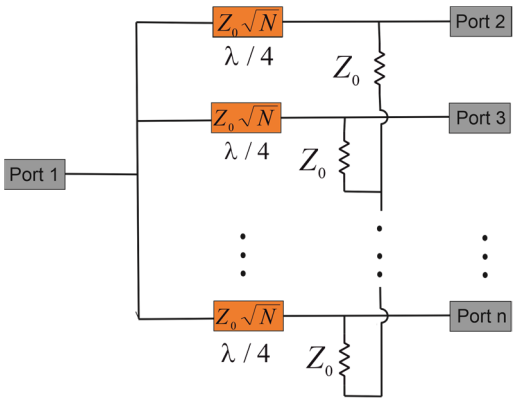

Figure 3. Conventional 1-to-N-way WPD.

Equivalent circuit models for conventional 2-, 4-, and 8-way cascaded WPDs are illustrated in Figure 4a–c, respectively. As can be seen from Figure 4, conventional 2-way WPDs comprise 2 quarter-wavelength $(\lambda/4)$ transmission lines with the characteristic impedances of $Z_0\sqrt{2}$. The same transmission line length and impedance values are also valid for 4- and 8-way WPDs, as depicted in Figure 4b,c. In order to obtain high isolation between the output ports, an isolation resistor of $2Z_0$ is connected between 2 output ports.

In addition, the input/output ports must have characteristic impedances of Z_0 for good impedance matching [28].

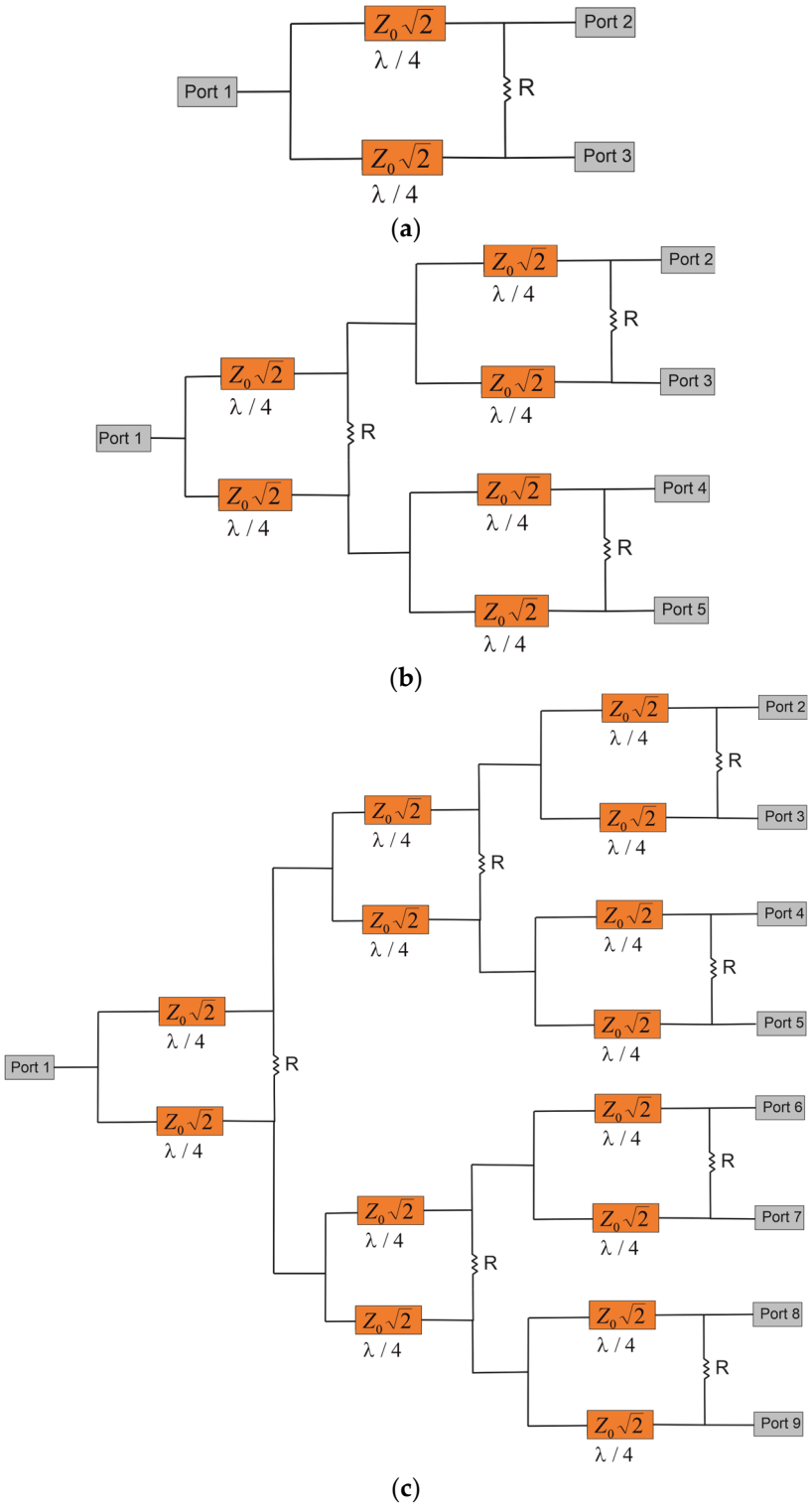

Figure 4. Conventional cascaded WPDs: (**a**) 2-way; (**b**) 4-way; (**c**) 8-way.

In order to reduce the overall circuit size, quarter-wavelength transmission lines can be capacitively or inductively loaded by different approaches, as shown in Figure 5. Due to the increase in the capacitance or inductance per unit length of the transmission line, the phase velocity on it decreases, so such a transmission line can be called a slow-wave

structure. Among the slow-wave structures shown in Figure 5, slit-loaded and meandered transmission lines are widely preferred for different kinds of microwave circuits because of their easy fabrication processes. However, the fabrication of interdigital capacitor-loaded transmission lines are more difficult than the others since they may need extra via connections. The number of narrow slits and meandered sections can be determined with respect to the desired center frequency. Here, it should be taken into consideration that a transmission line with narrow slits and meandered sections should exhibit similar behavior to a quarter-wavelength transmission line having the characteristic impedance of $Z_0\sqrt{2}$. Thus, the designed WPD would have optimum performance in terms of return loss and isolation. For this purpose, all dimensions and the number of narrow slits and meandered sections were determined by using the parameter sweep in Sonnet Software. Investigations into the related parameters are described in the following sections.

(**a**) (**b**) (**c**)

Figure 5. Slow-wave structures. (**a**) Slit-loaded. (**b**) Meandered. (**c**) Interdigital.

2.2.1. WPDs with Narrow-Slit-Loaded Transmission Lines

A 2-way WPD was constructed by loading narrow slits as shown in Figure 6 [28]. An RT/Duroid substrate with a relative dielectric constant of 10.2 and a thickness of 1.27 mm was used in all design processes. The number of slits and the location of the isolation resistor affect the frequency response as depicted in Figure 7a,b, respectively. It is clear that the center frequency decreases as the number of narrow slits increases. Therefore, a very compact size can be achieved by using the maximum number of slits. Since 50-ohm port impedances were utilized, the isolation resistor was chosen as 100 ohm.

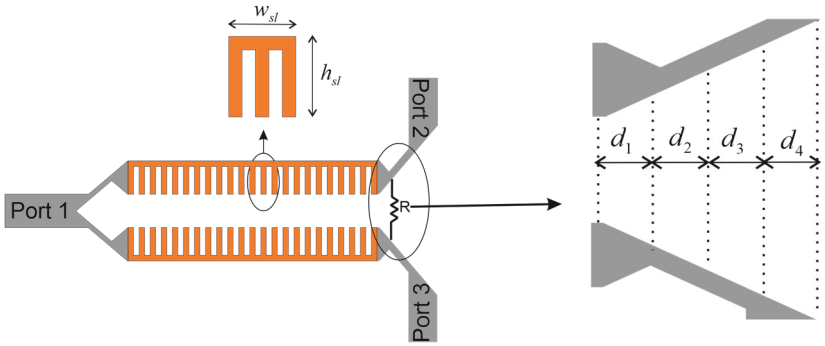

(**a**) (**b**)

Figure 6. (**a**) Conventional 2-way WPD-loading with narrow slits, and (**b**) location of the isolation resistor.

The proposed slit-loaded transmission lines in [28] were also used to design 4- and 8-way WPDs. Figure 8 illustrates the layouts of the 4- and 8-way WPDs in a cascaded model. It is clear that 2 more paths have been added instead of output ports for the 4- and 8-way power dividers.

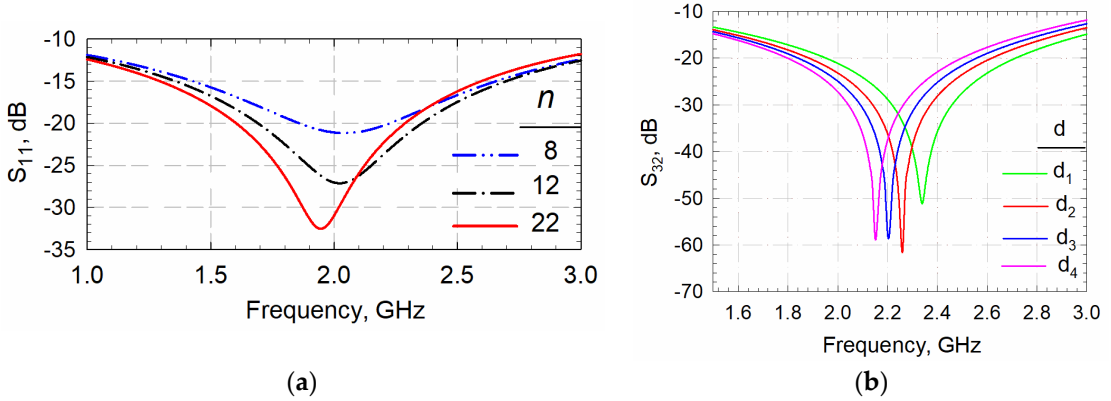

(**a**) (**b**)

Figure 7. (**a**) Effects of narrow slits on the frequency response. (**b**) Effects of locations of the isolation resistor on the frequency response.

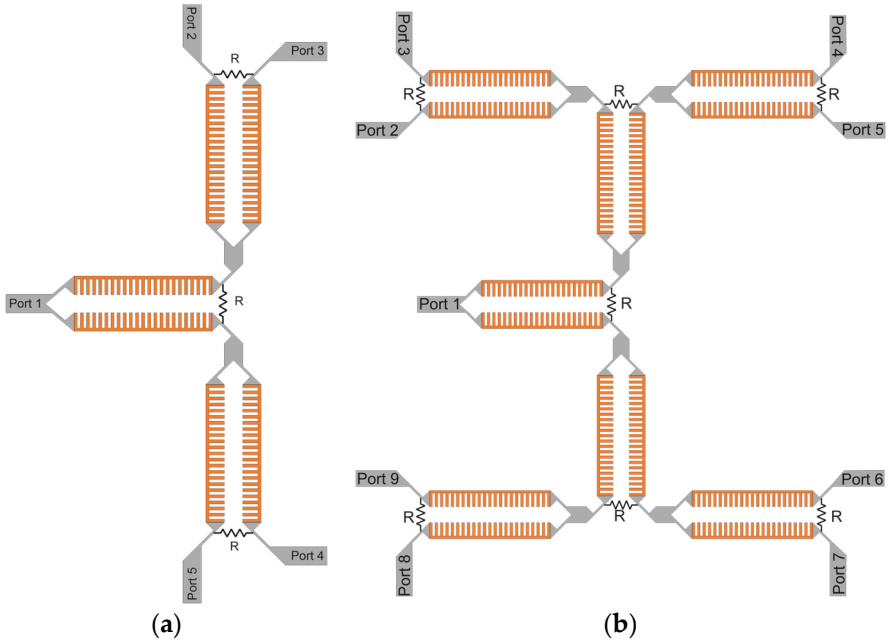

(**a**) (**b**)

Figure 8. (**a**) Four-way WPD loading with narrow slits. (**b**) Eight-way WPD loading with narrow slits.

2.2.2. WPDs with Meandered Transmission Lines

The meandered line model taken into consideration in this paper is shown in Figure 9. According to the even or odd number of meandered sections, the equivalent circuit model is depicted in Table 1 [29].

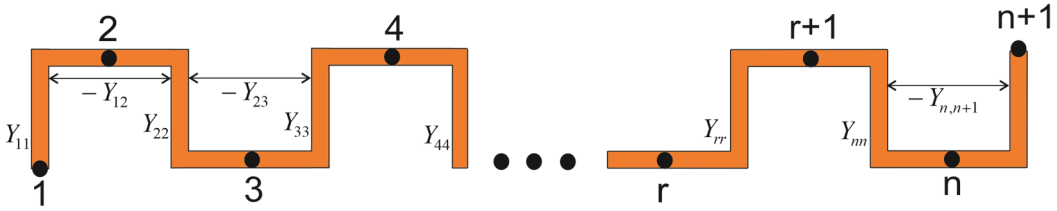

Figure 9. Meandered line model.

Table 1. Meandered line models and their equivalent circuits.

Odd line		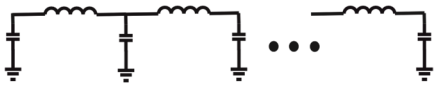
Even line	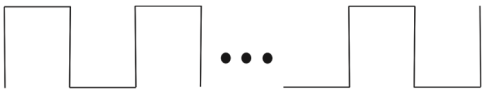	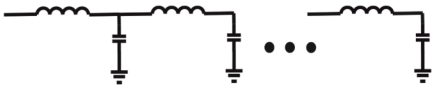

In a similar manner to the slit-loaded transmission lines, meandered sections can also be used for size reduction. Figure 10a illustrates a 2-way cascaded WPD constructed by meandered transmission lines. An RT/Duroid substrate with a relative dielectric constant of 10.2 and a thickness of 1.27 mm was used in all design processes. Effects of the number of meandered sections on the frequency response are depicted in Figure 10b. Here, the number of meandered sections is changed, starting from the middle of the transmission line. Depending on the proposed approach, a size reduction of 20.14% can be achieved.

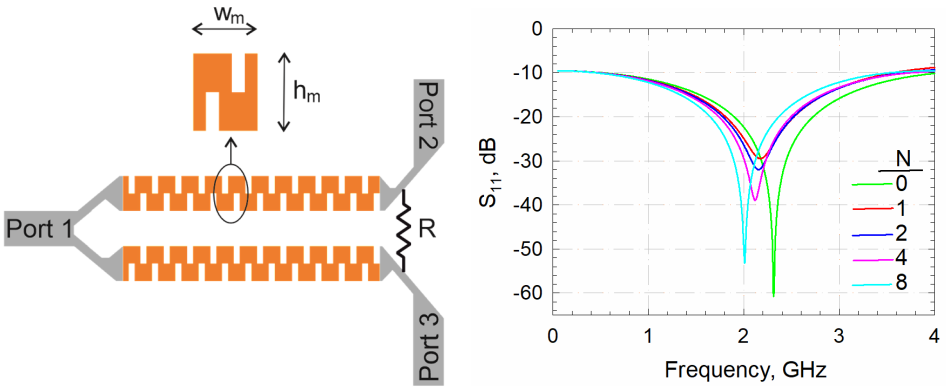

(**a**) (**b**)

Figure 10. (**a**) Conventional 2-way WPD having meandered transmission lines. (**b**) Effects of WPD meandering on the frequency response.

In addition to 2-way WPDs, more than 2 power-dividing operations can be necessary for the antenna arrays to be used in multi-way systems. For this purpose, the designed 2-way WPDs can be enhanced to 4-and 8-way circuits by means of meandered transmission lines, as shown in Figure 11a,b. As can be seen from Figure 11a, two two-way WPDs were connected in cascade for the four-way design. In this case, two reflection zeros can be observed since there are two identical transmission lines. In the eight-way WPDs, three reflection zeros appear due to the three cascaded transmission lines shown in Figure 11b. Here, the dimensions of the transmission lines, the isolation resistor and the resistor position are same as the 2-way WPDs. Accordingly, it is possible to achieve power-dividing operations in wider frequency bands by using more cascaded sections. The size reductions for the proposed 4- and 8-way power dividers are 16.62% and 9.99%, respectively. Electrical lengths of the proposed 2-, 4-, and 8-way WPDs are 0.20 λ_g × 0.078 λ_g, 0.56 λ_g × 0.25 λ_g, and 0.63 λ_g × 0.57 λ_g, respectively, where λ_g is the guided wavelength at the center frequency. Frequency responses of the designed circuits are given with the experimental studies in the following section.

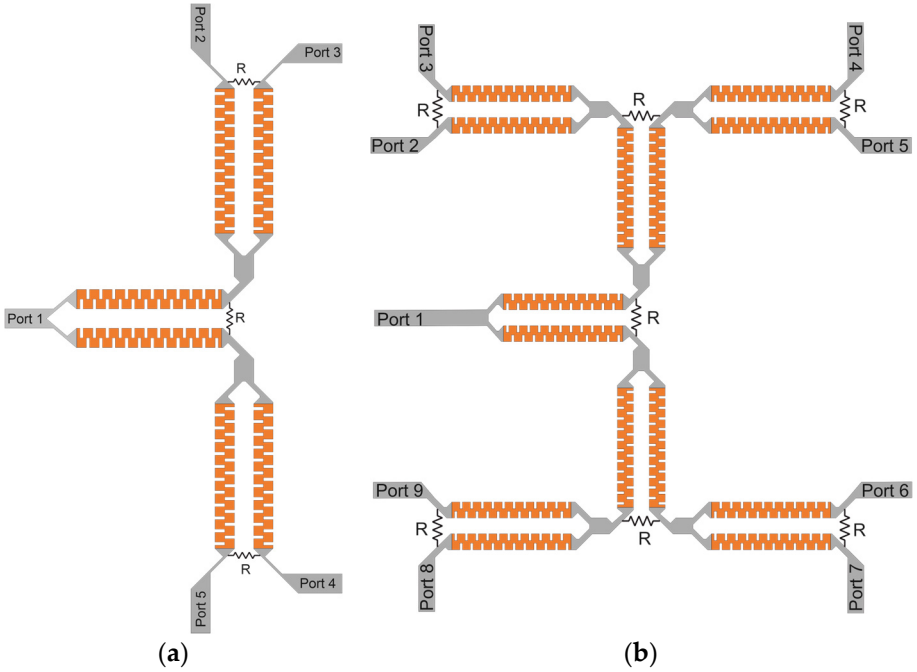

Figure 11. Conventional WPDs with meandered transmission lines: (**a**) 4-way; (**b**) 8-way.

2.2.3. Alternative Input/Output Port Arrangements for Various Power-Division Processes

In order to introduce various types of WPDs to be used for different feeding schemes of antenna arrays, new WPD configurations with different power-division ratios and input/output port arrangements were proposed by using meandered transmission lines. For this purpose, 3 different circuit topologies, including 3-way, 3-way double-layer, and 5-way double-layer WPDs were proposed. The main challenge of the proposed circuits is their power-halving property. Hence, the input power is halved at the next output ports and equal power-dividing ratios are achieved at the last two output ports.

Figure 12 illustrates the circuit for two three-way WPDs located at the same side of the board. As can be seen from Figure 12a, there are two input ports located at the upper left and bottom right. The upper output ports belong to the upper circuit, whereas the bottom output ports are for the bottom circuit. Both these WPDs perform the same operations in different paths, so the proposed arrangement actually behaves like a power-divider bank to be used for a multi-input—multi-output (MIMO) system. They are useful for different antenna arrays serving different operations. Moreover, the input power is halved at output port 2, while the power at output ports 3 and 4 is equal. The simulated frequency responses are demonstrated in Figure 12b. The magnitude and phase differences are also shown in Figure 12c,d, respectively.

The second WPD configuration was created for double-layer applications, as shown in Figure 13a. Here, a common ground plane was located between two layers, where both layers included two three-way power dividers for utilization in MIMO systems. The power divider in the upper layer is completely similar to the one in the bottom layer, so the proposed approach can be useful for bidirectional MIMO systems. The bottom and upper power dividers exhibit similar circuit performances. The S parameters of one of the two proposed WPDs are given in Figure 13b. Figure 13c,d represent the simulated magnitude and phase differences, respectively.

The last configuration was a 5-way WPD, as shown in Figure 14a. As can be seen from the figure, two layers were combined so as to have a common ground plane. The input port was located at the upper layer, and there were five output ports for power splitting. Two of the outputs are in the upper layer, whereas the remaining ports are in the bottom layer. The designed 5-way WPD halves the input power at the next port in a similar manner to the previous configuration. Hence, port 2 has 1/2, port 3 has 1/4, port 4 has 1/8, and

ports 5 and 6 both have 1/16 of the input power. This phenomenon can be seen from the simulated frequency responses shown in Figure 14b. The $|S_{21}|$, $|S_{31}|$, $|S_{41}|$, $|S_{51}|$, and $|S_{61}|$ parameters were approximately 3, 6, 9, 12, and 12 dB at the center frequency, respectively. Figure 14c,d show the magnitude and phase difference of the simulated S parameters.

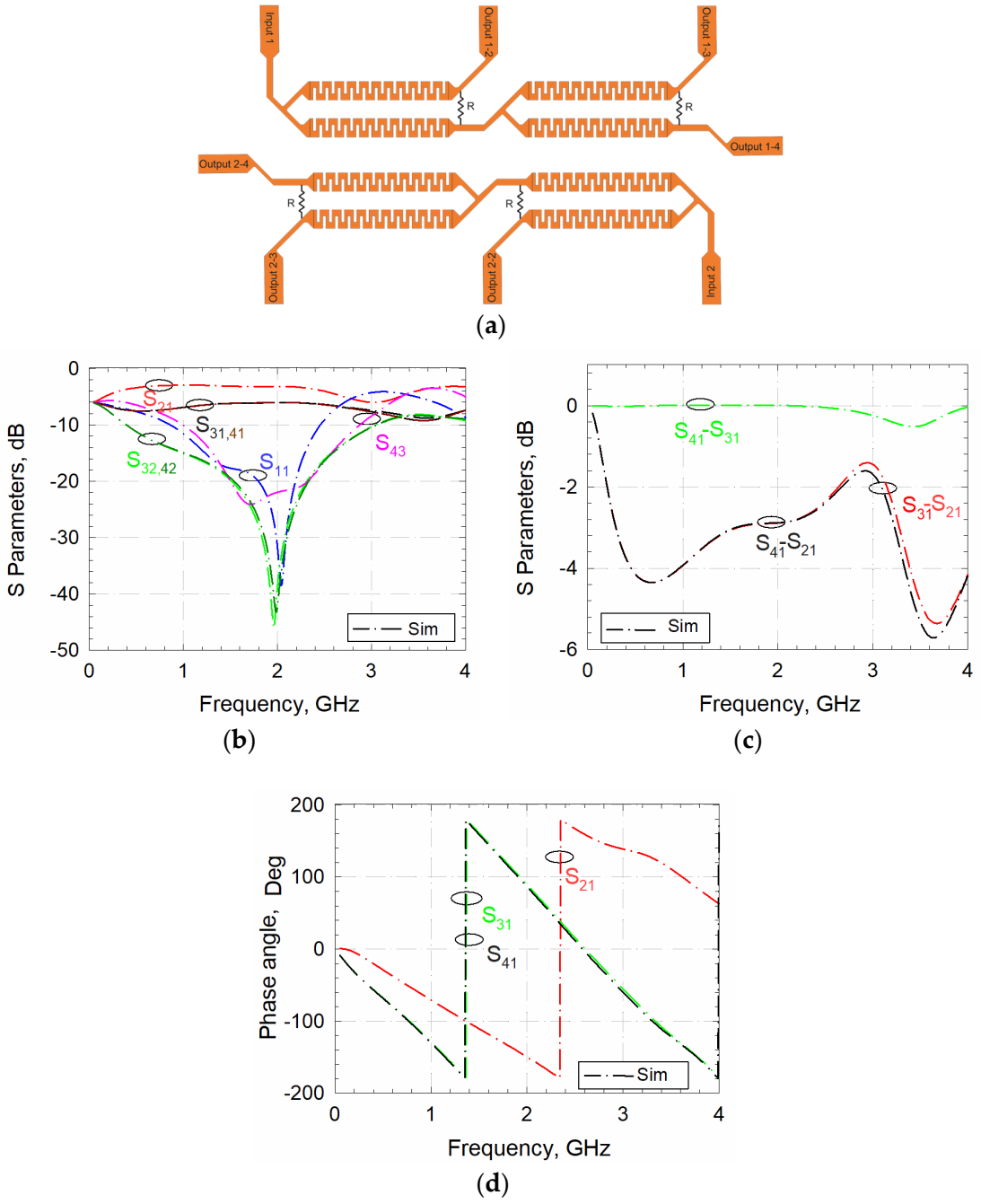

Figure 12. (**a**) Two 3-way WPDs with different inputs and outputs: (**b**) simulation results, (**c**) magnitude differences of S-parameters, and (**d**) phase responses.

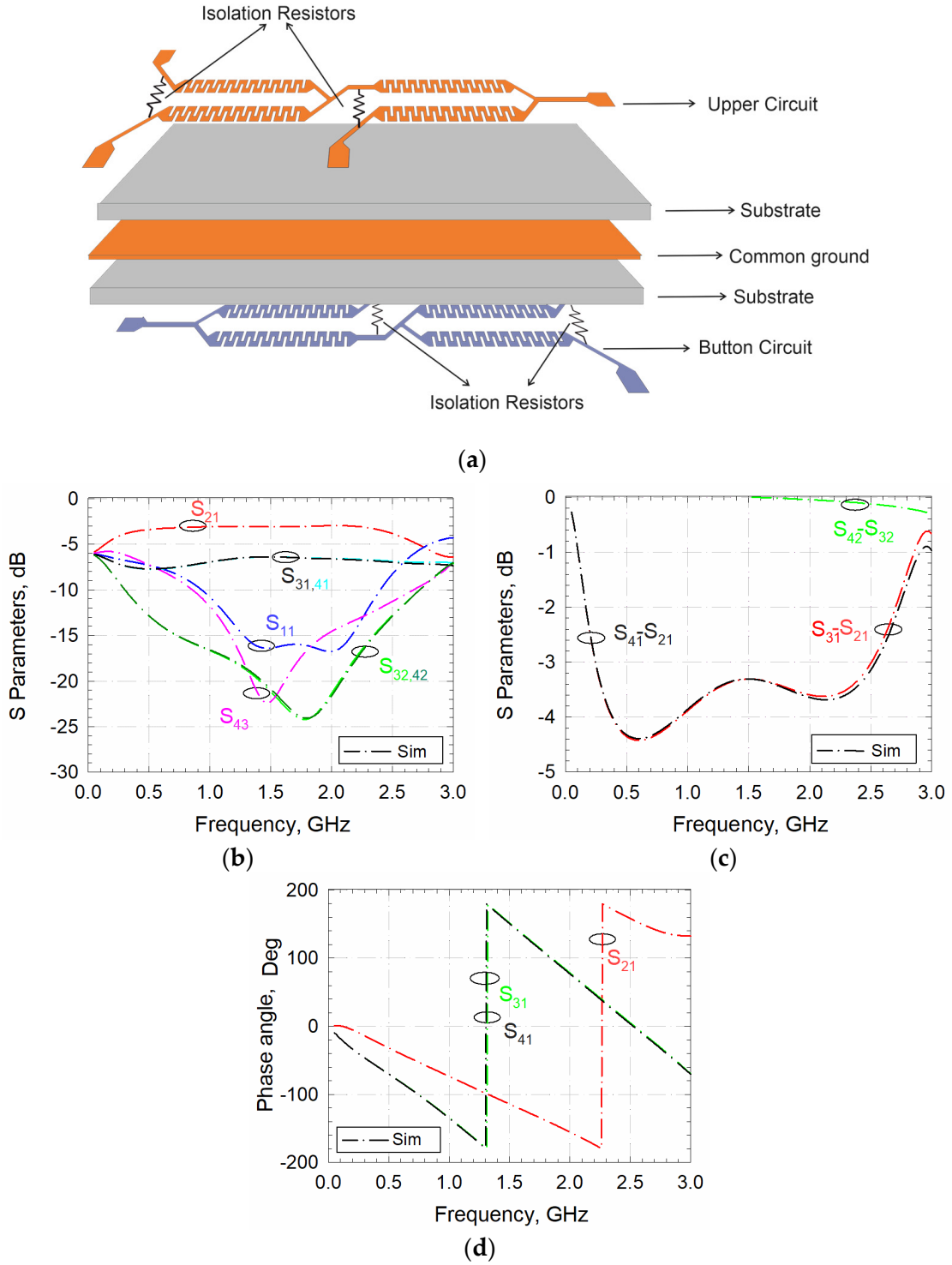

Figure 13. (**a**) Two 3-way WPDs with a common ground plane: (**b**) simulation results, (**c**) magnitude differences of S-parameters, and (**d**) phase responses.

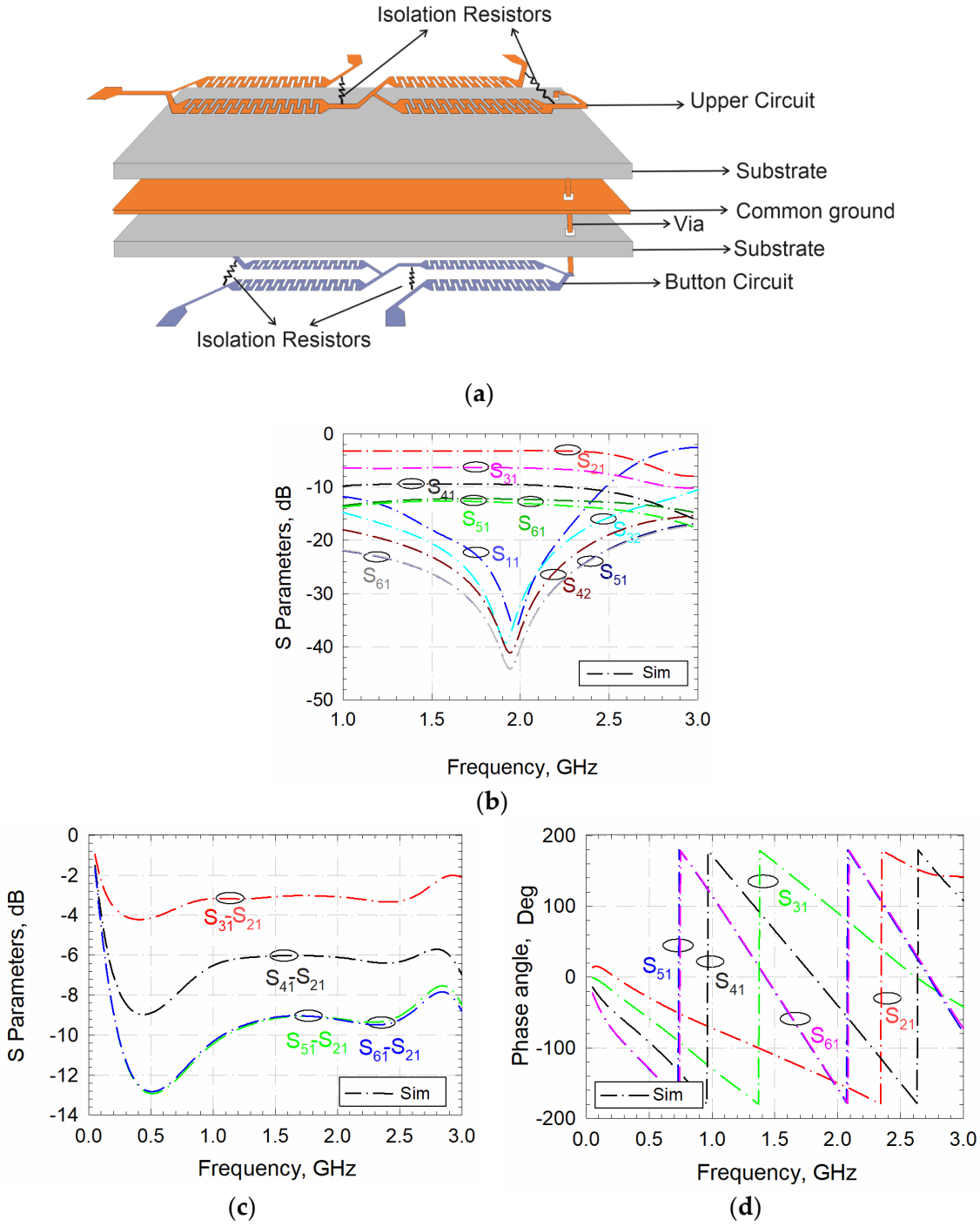

Figure 14. (**a**) Layout of a 5-way dual-layer WPD: (**b**) simulation results, (**c**) magnitude differences of S-parameters, and (**d**) phase responses.

3. Results

To demonstrate the proposed approaches, all the circuits designed with narrow-slit-loaded and meandered transmission lines were fabricated and tested. All circuits were simulated by using a full-wave electromagnetic simulator, Sonnet.

First, experimental studies of the power dividers having narrow-slit-loaded transmission lines introduced in [28] are presented. Photographs of the manufactured N-way WPDs having narrow slits in [28] are shown in Figure 15. Figure 16 illustrates a measurement view, where 50-ohm loads were used to match the idle output ports for 4- and 8-way power dividers since the measurement device has only four ports. The measured results of the

power dividers having narrow-slit-loaded transmission lines were compared with the simulated results in Figure 17 [28]. It is obvious that the measured and simulated results are in very good agreement. In Figure 17a, the center frequency was 2 GHz at the 15 dB fractional bandwidth (FBW) of 36.26%. As can be seen from the figure, the return loss and isolation level were better than 15 and 20 dB within the FBW, respectively. Within the FBW, the minimum isolation level and insertion loss were approximately 29.56 dB at 2 GHz and 3.29 dB, respectively. The measured and simulated results of the 4-way WPD are illustrated in Figure 17b, with the return loss and isolation level of better than 15 and 20 dB, respectively. The center frequency was 1.8 GHz at the FBW of 94.44%, and the insertion loss was better than 3 + 0.5 dB. Moreover, the center frequency of the 8-way WPD was measured at 1.9 GHz at the FBW of 81.05%. The measured results were compared with the simulated ones in Figure 17c, where the insertion loss, return loss, and isolation level obtained were better than 9 + 0.5, 15, and 20 dB, respectively.

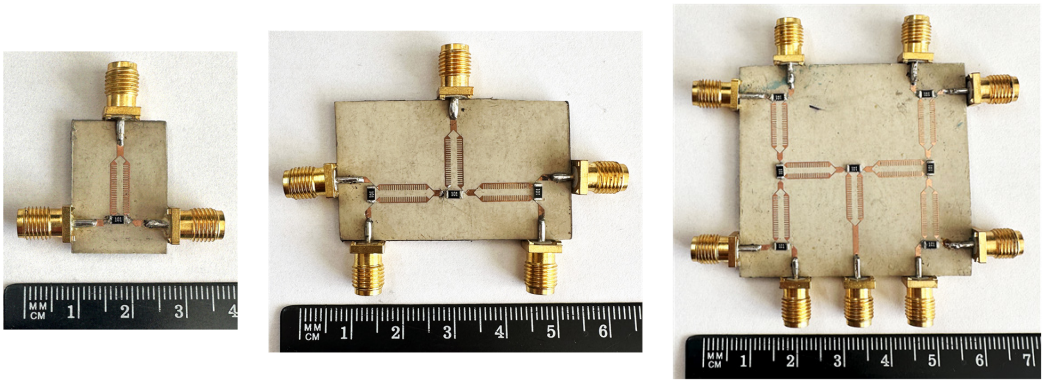

(**a**) (**b**) (**c**)

Figure 15. Photographs of N-way WPDs with narrow-slit-loaded transmission lines: (**a**) 2-way; (**b**) 4-way; and (**c**) 8-way.

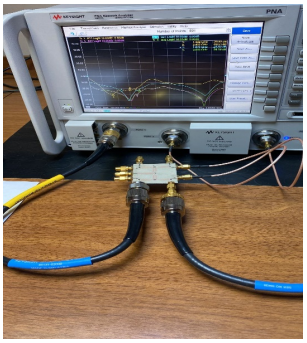

Figure 16. Measurement setup for an 8-way WPD.

Meandered-transmission-line-based two-, four-, and eight-way WPDs were also manufactured and tested. Photographs of the fabricated circuits are shown in Figure 18. The simulated and measured frequency responses for the 2-way WPD are compared in Figure 19a, where the return loss and isolation level are better than 15 and 30 dB, respectively. Frequencies of the minimum isolation and return loss levels are different because of fabrication errors. The measured center frequency was 2 GHz at the FBW of 75%. It should also be noted that there was only one reflection zero within the related frequency band. The measured magnitude and phase difference can be observed from Figure 19b,c, respectively. The center frequency of the 4-way power divider was measured at 1.77 GHz at the FBW of 73.09% as depicted in Figure 19a. At that frequency, the measured return and insertion losses were 24 and 3.1 dB, respectively. Isolation levels between the output ports were measured as better than 26 dB. In the frequency response of the four-way power divider,

there are two reflection zeros, since the circuit is composed of two cascaded sections. The measured magnitude and phase differences are also shown in Figure 20b,c, respectively. The simulated and measured results of the eight-way WPD are compared in Figure 21a and were found to be in very good agreement. In this case, three reflection zeros can be observed due to the utilization of three cascaded sections. The center frequency was measured at 1.73 GHz at the 15 dB FBW of 87.86%. Isolation levels between the output ports were better than 15 dB, 26 dB, 24 dB within the FBW, where the minimum insertion losses were 3.6 dB, 6.5, and 9.6 for 2-, 4-, and 8-way WPDs, respectively. The measured magnitude differences are shown in Figure 21b, with acceptable values smaller than 1 dB, and the phase differences can be observed in Figure 21c.

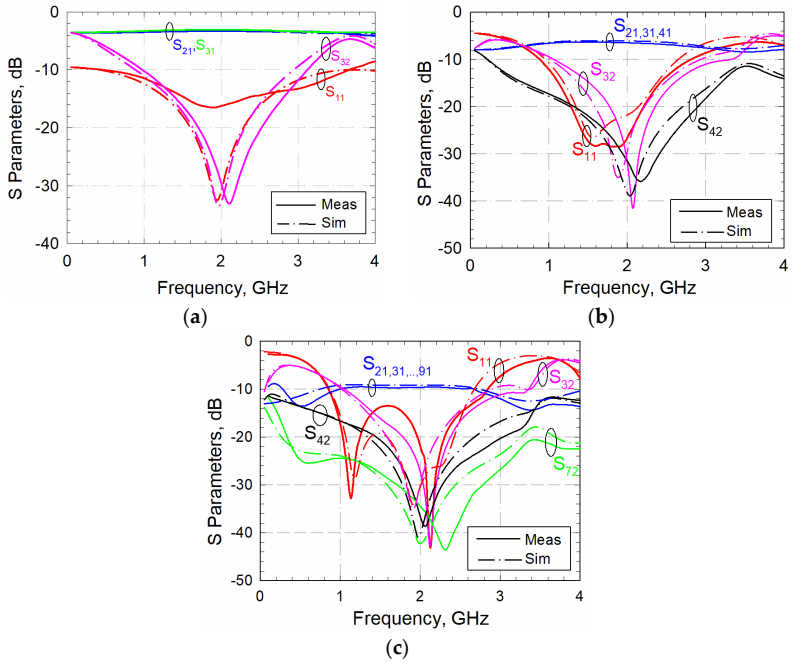

Figure 17. Comparison of the measured and simulated results of the WPDs having narrow-slit-loaded transmission lines for a (**a**) 2-way WPD; (**b**) 4-way WPD; and (**c**) 8-way WPD.

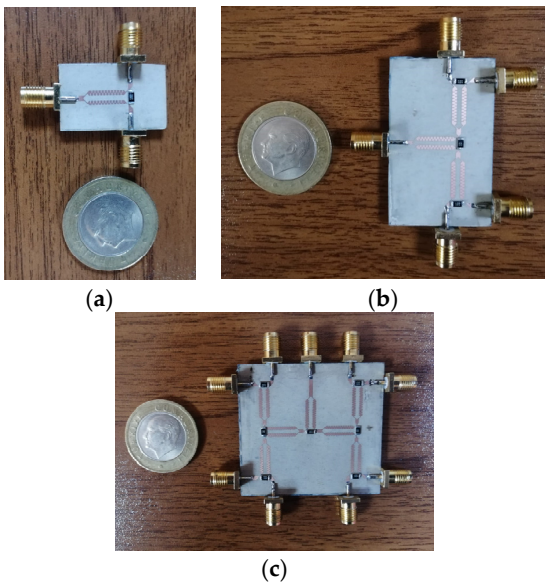

Figure 18. Meandered transmission line-based WPDs: (**a**) 2-way, (**b**) 4-way, and (**c**) 8-way.

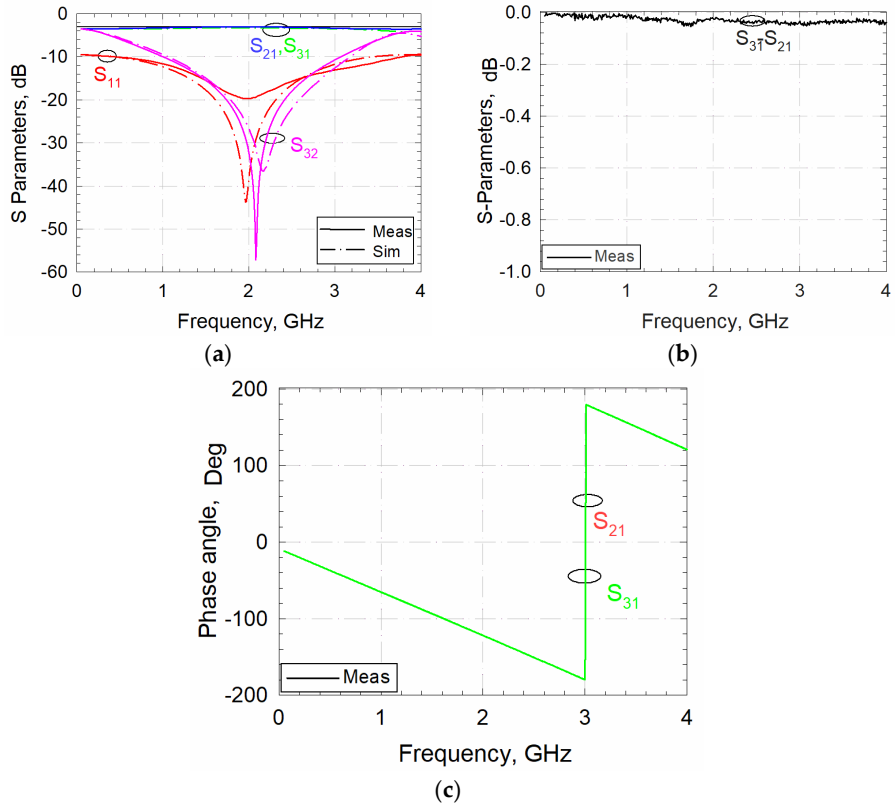

Figure 19. (**a**) Comparison of the measured and simulated results of the WPDs having meandered transmission lines for a 2-way WPD; (**b**) magnitude differences of S-parameters for a 2-way WPD; and (**c**) phase responses.

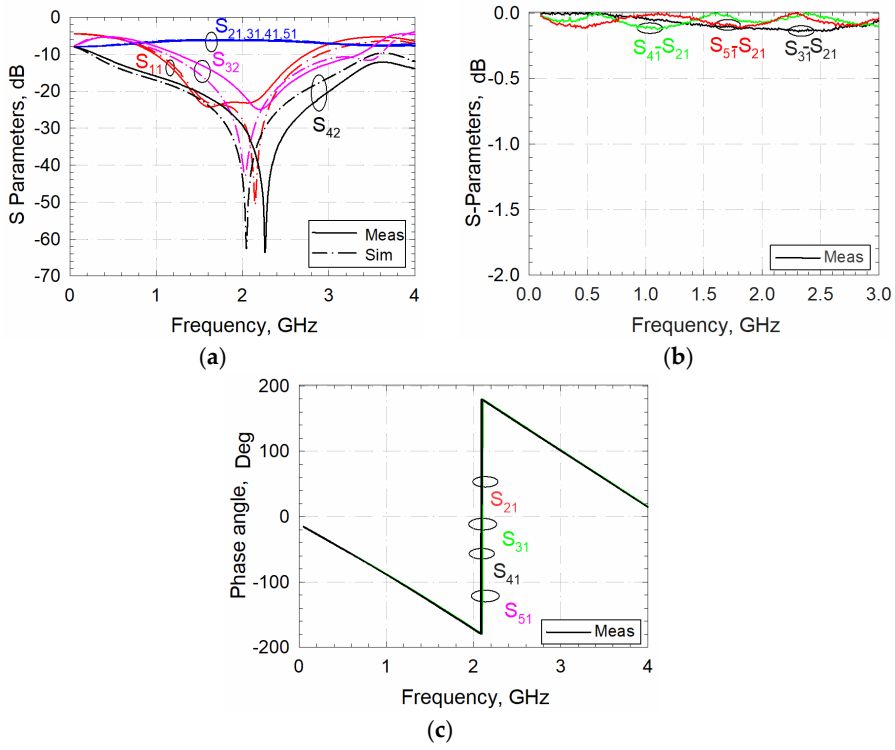

Figure 20. (**a**) Comparison of the measured and simulated results of the WPDs having meandered transmission lines for a 4-way WPD; (**b**) magnitude differences of S-parameters for a 4-way WPD; and (**c**) phase responses.

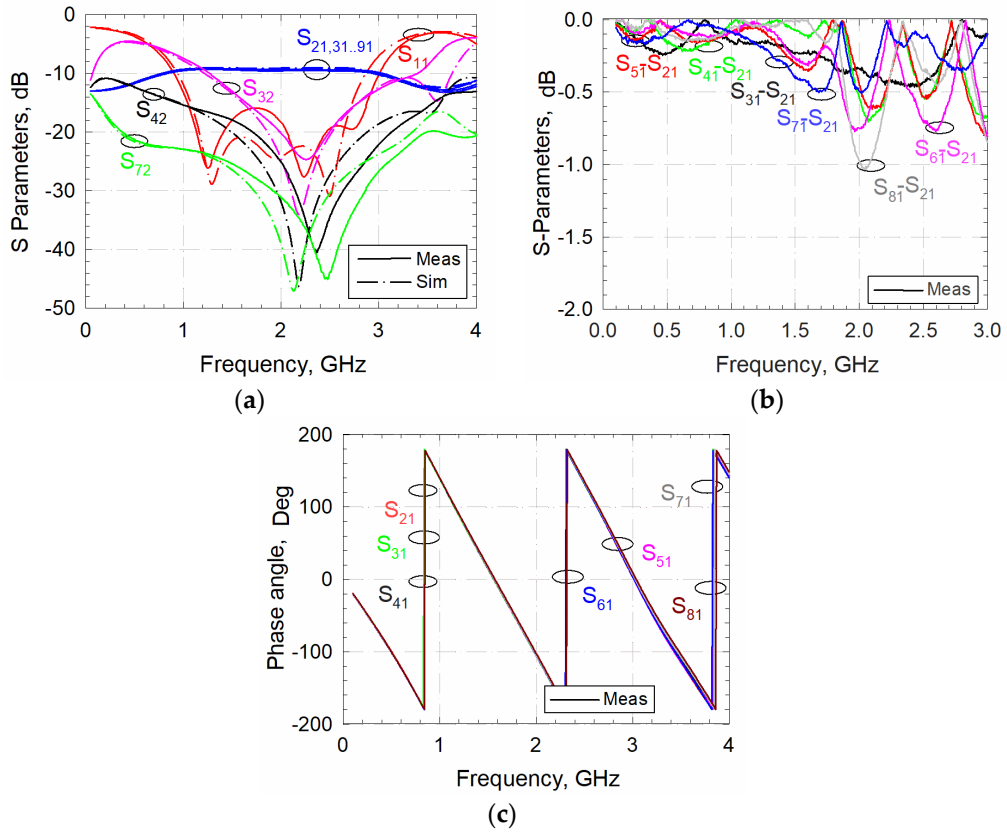

Figure 21. (**a**) Comparison of the measured and simulated results of the WPDs having meandered transmission lines for an 8-way WPD; (**b**) magnitude differences of S-parameters; and (**c**) phase responses.

Meandered-transmission-line-based WPDs with alternative input/output port configurations were manufactured and tested for demonstration. A photograph of the two fabricated three-way WPDs is shown in Figure 22a. The frequency response of the designed power divider is depicted in Figure 22b. As can be seen from the figure, the designed circuit can serve within the frequency band of 1.5–2.0 GHz. Within this frequency region, the isolation level between the output ports is better than 19.96 dB, the return loss is better than 17.71 dB, and the insertion loss is better than 3 + 0.5 dB. Figure 22c shows the magnitude differences, which are better than 4.4 dB. The phase responses corresponding to the S-parameters are also illustrated in Figure 22d.

The multilayer three-way WPD was implemented as shown in Figure 23a,b. It is obvious that the implemented circuit is different from the previous one, since two WPDs are located at both sides of the structure with a common ground plane. Comparisons of the simulated and measured results in terms of the return loss, insertion loss, and isolation level are depicted in Figure 23c. Within the frequency band of 1.5–2 GHz, the return loss was observed as better than 15 dB with an insertion loss of better than 3 + 0.5 dB at each output port. Furthermore, the isolation levels between all output ports were better than 19 dB. Figure 23d,e show the measured magnitude differences and phase responses, respectively. Unwanted differences for the measured results result from the fabrication errors which especially appeared during the combination of two layers. Two layers were combined by using copper tape to transfer the ground plane into the upper/down plane. Because of the small circuit size and the laboratory conditions, two circuit boards could not be combined by using screws.

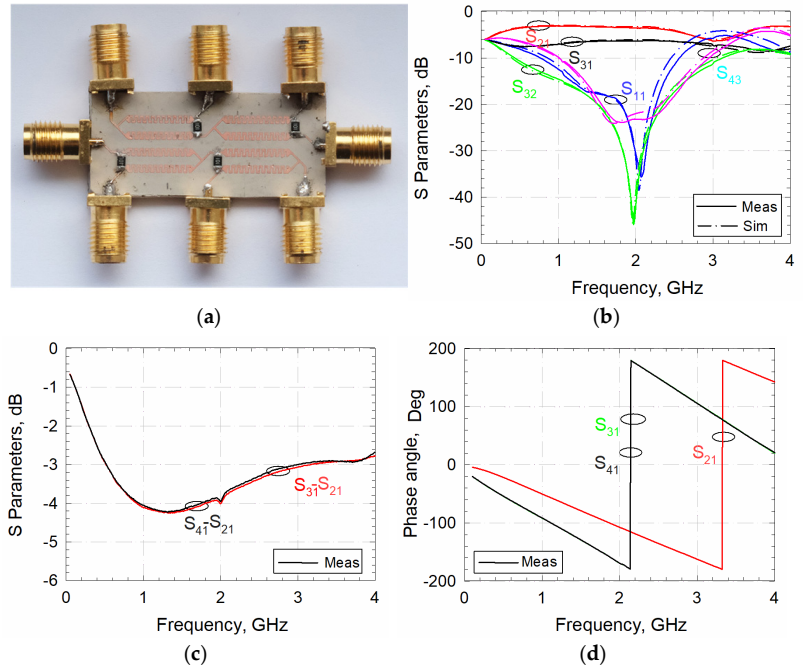

(**a**) (**b**) (**c**) (**d**)

Figure 22. (**a**) Photograph of the meandered transmission lines based on two three-way WPDs. (**b**) Measured and simulated S-parameters, (**c**) magnitude differences of S-parameters, and (**d**) phase responses.

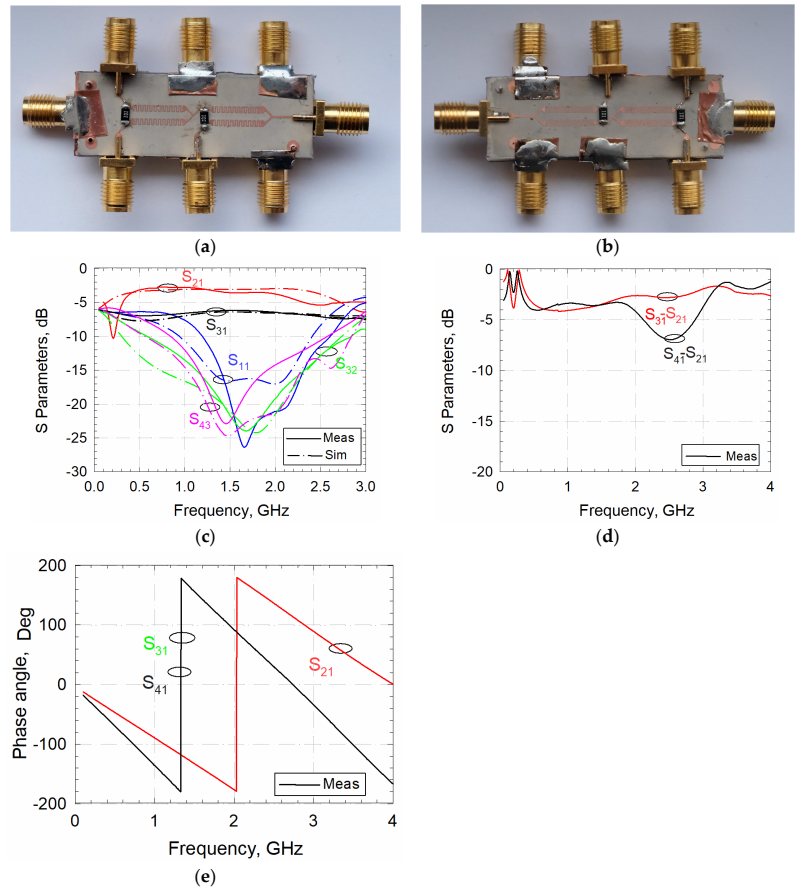

(**a**) (**b**) (**c**) (**d**) (**e**)

Figure 23. Meandered-transmission-line-based multilayer WPDs having a common ground plane: (**a**) front view, (**b**) back view. (**c**) Measured and simulated results. (**d**) Magnitude differences of S-parameters, and (**e**) phase responses.

A meandered-transmission-line-based multilayer five-way WPD was manufactured and successfully tested. Photographs of the front and back views of the fabricated circuits are shown in Figure 24a,b, respectively. The measured and simulated return and insertion losses of the proposed five-way power divider are compared in Figure 24c, with an acceptable agreement. The measured and simulated isolation levels between the output ports are also depicted in Figure 24d. It is clear that the proposed multilayer 5-way WPD can be used for different communication systems. Within the frequency band of 1.5–2 GHz, the return loss, insertion loss, and isolation levels are better than 16.52, 3 + 0.5, and 14.47 dB, respectively. The differences between the measured and simulated responses resulted from the fabrication errors and especially from the layer-combining process. Magnitude differences between the insertion losses and the phase responses are shown in Figure 24e,f, respectively.

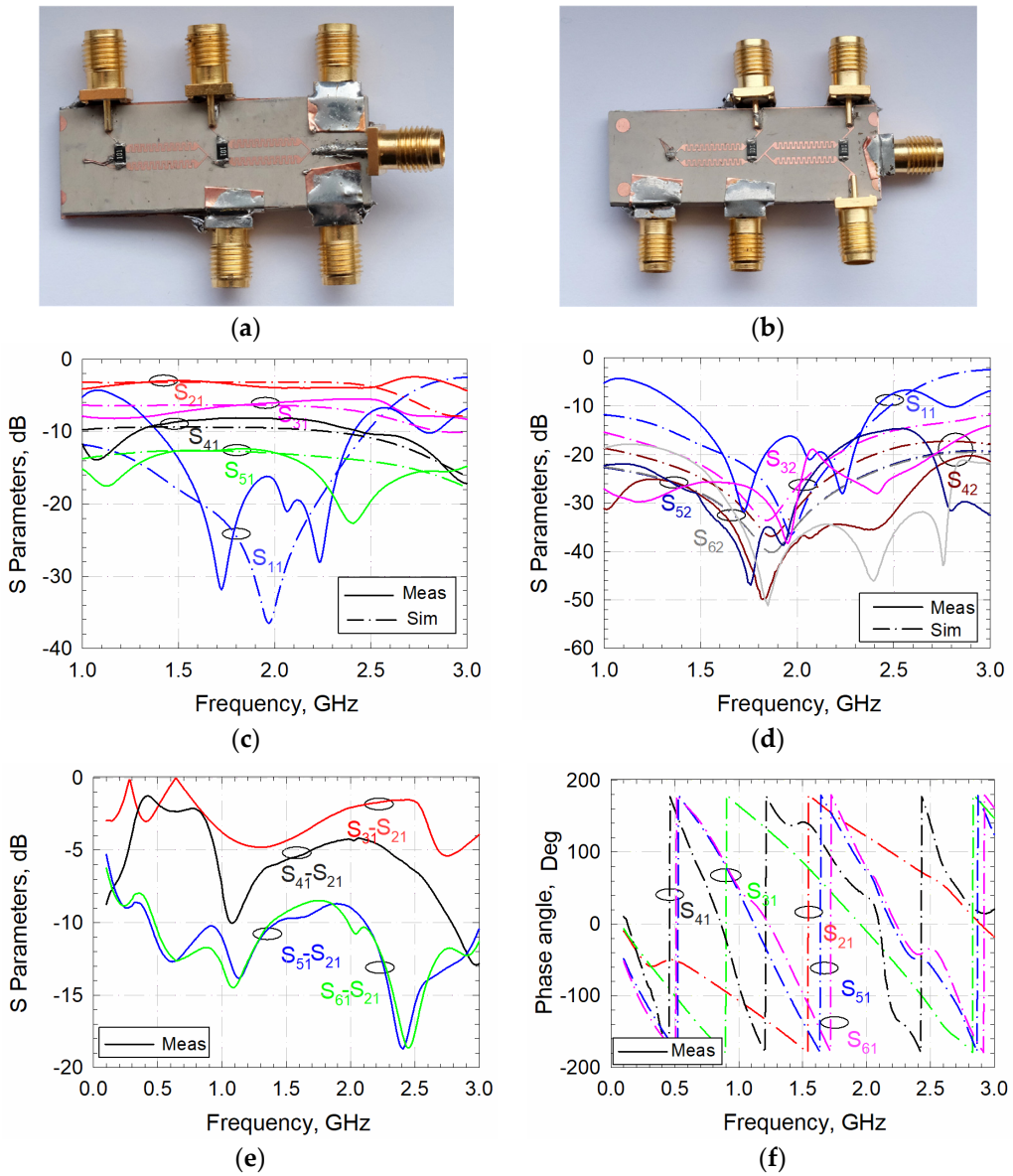

Figure 24. Meandered-transmission-line-based multilayer 5-way WPD: (**a**) front view and (**b**) back view. (**c**) Measured and simulated return and insertion losses and (**d**) isolation levels. (**e**) Magnitude differences of S-parameters and (**f**) phase responses.

Table 2 summarizes and compares the measurements of the proposed designs with the work published in the literature. The proposed configurations in this work introduce WPDs with new input/output configurations that may be used in front of antenna arrays to

be used for different personal and mobile communication systems. For this purpose, WPDs based on single- and dual-layer slow-wave structures providing equal power division have been introduced for the first time in this paper. The proposed circuits in this work also have promising circuit sizes.

Table 2. Performance comparison of the proposed WPD with previous works.

Ref	f_o (GHz)	Size (λ_g^2)	FBW (%)	Structure Topology
[2]	1.32	-	103.60	Three-section TL lines & three resistors
[6]	2.1	0.6386	80	Two-stage with coupled lines
[10]	2.6	0.096	18.2	ITPD
[28]	2	0.0156	36.26	Slit-loaded transmission lines
Meandered line (this work)	2.03	0.0156	56.79	Meandered transmission lines
3-way WPDs (this work)	1.95	0.12	52.5	Microstrip transmission lines
3-way WPDs with common ground plane (this work)	1.74	0.079	52.29	Microstrip transmission lines
5-way WPDs with common ground plane (this work)	1.97	0.073	51.26	Microstrip transmission lines

4. Conclusions

In this study, various types of WPDs have been developed and experimentally investigated by using slow-wave structures. For this purpose, WPDs having narrow-slit-loaded transmission lines were investigated, and novel meandered-transmission-line-based WPDs were introduced for the first time. The proposed meandered-line-based two-, four-, and eight-way power dividers have been fabricated and measured successfully. The proposed meandered transmission lines have also been used to design new types of WPDs with new input/output port arrangements. In this context, two three-way WPDs have been located on the same plane for similar power-splitting processes. Next, this circuit has been developed by locating one of the power dividers to another layer. The proposed circuits can behave like a power-divider bank to be used for alternative antenna array applications. Moreover, a five-way WPD has been designed by using meandered transmission lines in two layers. These alternative WPD topologies allow halving of the input power at the next output port. These WPDs have been implemented and their measurements show an acceptable agreement with the simulated results.

Author Contributions: Conceptualization, M.C., A.K.G., C.K. and A.G.; methodology, M.C., A.K.G., C.K. and A.G.; software, M.C., A.K.G., C.K. and A.G.; validation, M.C., A.K.G., C.K. and A.G.; investigation, M.C., A.K.G., C.K. and A.G.; resources, M.C., A.K.G., C.K. and A.G.; writing—original draft preparation, M.C., A.K.G., C.K. and A.G.; writing—review and editing, M.C., A.K.G., C.K. and A.G.; visualization, M.C., A.K.G., C.K. and A.G.; supervision, C.K. and A.K.G.; project administration, A.G. All authors have read and agreed to the published version of the manuscript.

Funding: This work was supported by the Scientific and Technological Research Council of Turkey (TUBITAK) under Grant 120E101.

Institutional Review Board Statement: Not applicable.

Informed Consent Statement: Not applicable.

Data Availability Statement: Data and simulation files will be shared upon request from the authors.

Conflicts of Interest: The authors declare no conflict of interest.

Abbreviation

S_{mm}	Reflection coefficient at port m.
S_{mn}	Transmission coefficient from port n to port m.
WPD	Wilkinson power divider.
Meas	Measured.
Sim.	Simulated.
f_0	Center frequency.
FBW	Fractional bandwidth.
λ_g	Guided wavelength.

References

1. Razzaz, F.; Saeed, S.M.; Alkanhal, M.A.S. Compact Ultra-Wideband Wilkinson Power Dividers Using Linearly Tapered Transmission Lines. *Electronics* **2022**, *11*, 3080. [CrossRef]
2. Omi, A.I.; Zafar, Z.N.; Al-Shakhori, H.; Savage, A.N.; Islam, R.; Maktoomi, M.A.; Zakzewski, C.; Sekhar, P. A new analytical design methodology for a three-section wideband wilkinson power divider. *Electronics* **2021**, *10*, 2332. [CrossRef]
3. Gao, N.; Wu, G.; Tang, Q. Design of a novel compact dual-band wilkinson power divider with wide frequency ratio. *IEEE Microw. Wirel. Compon. Lett.* **2014**, *24*, 81–83. [CrossRef]
4. Khajeh-Khalili, F.; Honarvar, M.A.; Virdee, B.S. Miniature In-Phase Wilkinson Power Divider with Pair of Parallel Transmission-Lines for Application in Wireless Microwave Systems. *IETE J. Res.* **2018**, *67*, 227–234. [CrossRef]
5. Khajeh-Khalili, F.; Honarvar, M.A. A design of triple lines Wilkinson power divider for application in wireless communication systems. *J. Electromagn. Waves Appl.* **2016**, *30*, 2110–2124. [CrossRef]
6. Saxena, A.; Hashmi, M.; Banerjee, D.; Chaudhary, M.A. Theory and design of a flexible two-stage wideband wilkinson power divider. *Electronics* **2021**, *10*, 2168. [CrossRef]
7. Liang, W.-F.; Hong, W.; Chen, J.-X. A Q-band compact Wilkinson power divider using asymmetrical shunt-stub in 90nm CMOS technology. In Proceedings of the 2012 Asia Pacific Microwave Conference Proceedings, Kaohsiung, Taiwan, 4–7 December 2012; pp. 974–976. [CrossRef]
8. Khajeh-Khalili, F.; Honarvar, M.A.; Limiti, E. A Novel High-Isolation Resistor-Less Millimeter-Wave Power Divider Based on Metamaterial Structures for 5G Applications. *IEEE Trans. Compon. Packag. Manuf. Technol.* **2020**, *11*, 294–301. [CrossRef]
9. Kawai, T.; Nagano, K.; Enokihara, A. Dual-Band Semi-Lumped-Element Power Dividers at UHF/SHF Bands. In Proceedings of the 50th European Microwave Conference, EuMC, Utrecht, The Netherlands, 12–14 January 2021; pp. 844–847.
10. Gupta, R.; Assaad, M.; Chaudhary, M.A.; Hashmi, M. An Effective Design Scheme of Single- and Dual-Band Power Dividers for Frequency-Dependent Port Terminations. *Electronics* **2023**, *12*, 1991. [CrossRef]
11. Wu, Y.; Liu, Y.; Zhang, Y.; Gao, J.; Zhou, H. A dual band unequal wilkinson power divider without reactive components. *IEEE Trans. Microw. Theory Tech.* **2009**, *57*, 216–222. [CrossRef]
12. Al Shamaileh, K.; Dib, N.; Abushamleh, S. A Dual-Band 1:10 Wilkinson Power Divider Based on Multi-T-Section Characterization of High-Impedance Transmission Lines. *IEEE Microw. Wirel. Compon. Lett.* **2017**, *27*, 897–899. [CrossRef]
13. Lee, S.; Park, J.; Hong, S. Millimeter-Wave Multi-Band Reconfigurable Differential Power Divider for 5G Communication. *IEEE Trans. Microw. Theory Tech.* **2022**, *70*, 886–894. [CrossRef]
14. Okada, Y.; Kawai, T.; Enokihara, A. Design Method for Multiband WPDs Using Multisection LC-Ladder Circuits. *IEEE Microw. Wirel. Compon. Lett.* **2017**, *27*, 894–896. [CrossRef]
15. Gomez-Garcia, R.; Loeches-Sanchez, R.; Psychogiou, D.; Peroulis, D. Single/multi-band Wilkinson-type power dividers with embedded transversal filtering sections and application to channelized filters. *IEEE Trans. Circuits Syst. I Regul. Pap.* **2015**, *62*, 1518–1527. [CrossRef]
16. Scardelletti, M.C.; Ponchak, G.E.; Weller, T.M. Miniaturized Wilkinson power dividers utilizing capacitive loading. *IEEE Microw. Wirel. Compon. Lett.* **2002**, *12*, 6–8. [CrossRef]
17. Wu, J.; Li, E.; Guo, G.F. Microstrip power divider with capacitive stubs loading for miniaturization and harmonic suppression. In Proceedings of the ICMTCE2011-Proceedings 2011 IEEE International Conference on Microwave Technology and Computational Electromagnetics, Beijing, China, 22–25 May 2011; pp. 237–239.
18. Karpuz, C.; Gorur, A.K. Effects of narrow slits on frequency response of a microstrip square loop resonator and dual-mode filter applications. *Microw. Opt. Technol. Lett.* **2012**, *55*, 143–146. [CrossRef]
19. Santiko, A.B.; Munir, A. Development of dual band power divider using meander line technique for local oscillator system. In Proceedings of the IEEE 13th International Conference on Telecommunication Systems, Services, and Applications (TSSA), Bali, Indonesia, 3–4 October 2019; pp. 286–289.
20. Rawat, K.; Ghannouchi, F.M. A design methodology for miniaturized power dividers using periodically loaded slow wave structure with dual-band applications. *IEEE Trans. Microw. Theory Tech.* **2009**, *57*, 3380–3388. [CrossRef]
21. Park, M.J.; Lee, B. A dual-band Wilkinson power divider. *IEEE Microw. Wirel. Compon. Lett.* **2008**, *18*, 85–87. [CrossRef]
22. Kim, K.; Nguyen, C. An ultra-wideband low-loss millimeter-wave slow-wave wilkinson power divider on 0.18 μm SiGe BICMOS process. *IEEE Microw. Wirel. Compon. Lett.* **2015**, *25*, 331–333. [CrossRef]

23. Roshani, S.; Yahya, S.I.; Alameri, B.M.; Mezaal, Y.S.; Liu, L.W.Y.; Roshani, S. Filtering Power Divider Design Using Resonant LC Branches for 5G Low-Band Applications. *Sustainability* **2022**, *14*, 12291. [CrossRef]
24. Wang, Y.; Zhang, X.-Y.; Liu, F.-X.; Lee, J.-C. A Compact Bandpass Wilkinson Power Divider With Ultra-Wide Band Harmonic Suppression. *IEEE Microw. Wirel. Compon. Lett.* **2017**, *27*, 888–890. [CrossRef]
25. Sallam, T.; Attiya, A.M. Neural network inverse model for multi-band unequal Wilkinson power divider. *COMPEL-Int. J. Comput. Math. Electr. Electron. Eng.* **2022**, *41*, 1604–1617. [CrossRef]
26. Cheng, J.-D.; Xia, B.; Xiong, C.; Wu, L.-S.; Mao, J.-F. An Unequal Wilkinson Power Divider Based on Integrated Passive Device Technology and Parametric Model. *IEEE Microw. Wirel. Compon. Lett.* **2022**, *32*, 281–284. [CrossRef]
27. Peng, C.; Ye, Z.; Wu, J.; Chen, C.; Wang, Z. Design of a wide-dynamic rf-dc rectifier circuit based on an unequal wilkinson power divider. *Electronics* **2021**, *10*, 2815. [CrossRef]
28. Karpuz, C.; Gorur, A.K.; Cakir, M.; Cengiz, A.; Gorur, A. Compact Wilkinson Power Dividers Based on Narrow Slits Loaded Transmission Lines. In Proceedings of the 2023 IEEE Radio and Wireless Symposium (RWS), Las Vegas, NV, USA, 22–25 January 2023; pp. 174–177. [CrossRef]
29. Sato, R. A Design Method for Meander-Line Networks Using Equivalent Circuit Transformations. *IEEE Trans. Microw. Theory Tech.* **1971**, *19*, 431–442. [CrossRef]